ACS Biomaterials SCIENCE & ENGINEERING

pubs.acs.org/journal/abseba

Article

New Impedimetric Sandwich Immunosensor for Ultrasensitive and Highly Specific Detection of Spike Receptor Binding Domain Protein of SARS-CoV-2

Elif Burcu Aydın, Muhammet Aydın, and Mustafa Kemal Sezgintürk*

Cite This: *ACS Biomater. Sci. Eng.* 2021, 7, 3874−3885

Read Online

ACCESS | Metrics & More | Article Recommendations | Supporting Information

ABSTRACT: An impedance sensing platform-combined conducting nanocomposite layer was fabricated to develop an effective and rapid method for detection of coronavirus infection (COVID-19) specific spike receptor binding domain (RBD) protein, a precious antigen marker of COVID-19 disease. Coronavirus infection has spread globally and swiftly with major impacts on health, economy, and quality of life of communities. Fast and reliable detection of COVID-19 is a very significant issue for the effective treatment of this bad illness. For this aim, first, an Epoxy functional group-substituted thiophene monomer was synthesized and electrodeposited on a single-use indium tin oxide (ITO) platform in the presence of acetylene black by employing a cyclic voltammetry technique; thus, a conducting nanocomposite (*C-NC*) layer with high conductivity was obtained. This composite was electrodeposited for the first time on the ITO surface to generate a facile and cost-effective impedimetric biosensor. In addition, this composite provided proper attachment points for antibody binding and also supported the biosensor construction. The immuno-specific biointeractions between anti-RBD and RBD proteins hampered the electron transfer between the ITO substrate surface and electrolyte, and this reaction caused variations in impedance signals, and these signals were proportional to the immobilized RBD antigen amounts. The as-prepared immunosensor showed a wide linear dynamic range (0.0012−120 pg/mL), an ultra-low detection limit of 0.58 fg/mL with added superiorities of great selectivity, suitable repeatability, multiple reusability, and excellent reproducibility.

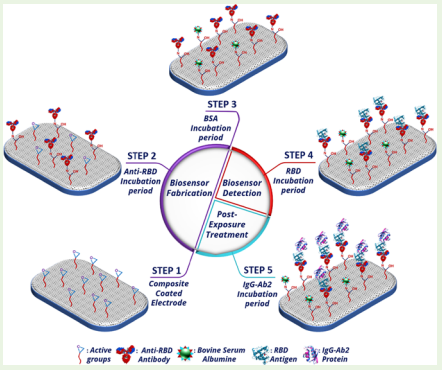

KEYWORDS: *spike receptor binding domain, conducting nanocomposite, impedimetric analysis, single-use electrode*

1. INTRODUCTION

At the end of the year 2019, an outbreak, which was originated from an unknown pathogen, was first observed in the city of Wuhan, China.[1] This pneumonia was associated with a coronavirus, which was known as severe acute respiratory syndrome coronavirus 2 (SARS-COV-2).[2] This outbreak has spread worldwide and caused fever and several respiratory illnesses.[3] The ongoing pandemic of SARS-COV-2 has resulted in more than 82,579,768 confirmed cases and 1,818,849 deaths as of 03 January 2021 (http://covids.who.int/). Therefore, rapid and reliable diagnosis of COVID-19 is very important.

SARS-COV-2 is the third largely pathogenic outbreak that infects humans and utilizes the same receptor, which is called angiotensin converting enzyme 2 (ACE 2), for cell entry.[4] Like other coronaviruses, the spike (S) glycoprotein homotrimer on the SARS-COV-2 surface has an important role in receptor attachment and virus entry. The "S" glycoprotein is a type I fusion protein, and each "S" protomer includes S1 and S2 domains with a receptor binding domain (RBD), which is encoded in the S1 domain.[5] The S1 subdomain attaches to the host receptor, and the S2 subdomain mediates membrane fusion.[6] It has been noticed in literature studies that SARS-Cov-2 codes four glycoproteins containing the spike, envelope, matrix, and nucleocapsid.[7,8] Among these structural glycoproteins, the spike protein (S) is a plentiful virus transmembrane protein, and it shows high immunogenicity.[9] Moreover, the amino acid order of this glycoprotein has variety from another coronaviruses. Spike protein is an appropriate protein for selective identity of SARS-CoV-2.[10,11] Therefore, screening of RBD as a target of COVID-19 virus is a priority.

During the early period of the SARS-CoV-2 outbreak, many COVID-19 infected patients are identified by using deoxyribonucleic acid (DNA) sequencing technology and the reverse transcription-polymerase chain reaction (RT-PCR) technique.[12] DNA sequencing technology can determine mutations and evaluate the SAR-CoV-2 isolates. Currently, three diagnostic methods are utilized for COVID-19 detection:

Received: April 29, 2021
Accepted: July 15, 2021
Published: July 22, 2021

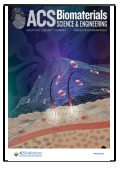

https://doi.org/10.1021/acsbiomaterials.1c00580
ACS Biomater. Sci. Eng. 2021, 7, 3874−3885

(1) Chest CT scan and clinical findings, (2) ribonucleic acid detection with RT-PCR, and (3) lateral flow immunoassay (LFA). The chest CT scan can be performed only in larger hospitals, and this method is not specific for COVID-19 detection. The RT-PCR technique requires 1−3 days to obtain results, and it possesses a high false-negative rate.[13] LFA is a portable and cheap point-of-care diagnostic tool and usually used for IgG and IgM protein detection.[14] Though the serological tests are cost-effective and require short time for analysis, they are not suitable for the diagnosis of COVID-19 at the early stage of infection because the detectable level of antibodies is produced at 10−14 days after infection. Because of this, low-cost and reliable sensing tools are required for rapid testing COVID 19.[15] Biosensors are effective biodevices for rapid, accurate, portable, and more promising diagnosis in the existing pandemic that has exaggerated the world humanity and economies. Optical biosensors, wearable biosensors, smart band, cell-based biosensors, plasmonic photothermal biosensors, and nanosensors have been developed to diagnose COVID-19. The results obtained from several studies in the literature illustrate that biosensors are successful tools with high sensitivity and specificity as well as fast performance that can be a good alternative to common methods of coronavirus detection. They are simple and cheap devices for COVID-19 pandemic screening.[16]

Different biosensors have been developed for spike RBD protein detection, and different fabrication protocols have been used in all systems. Cobalt-functionalized TiO_2 nanotube (Co-TNT)-based electrochemical sensing systems,[17] ACE2-receptor-modified LFA,[18] anti-S1 cell-based biosensors,[19] and 1-pyrene butyric acid *N*-hydroxysuccinimide ester-modified biosensing systems[20] have been utilized for spike RBD protein detection. The development strategies of these biosensors were longer, more complicated, and more laborious than the proposed biosensor. The proposed sensing system provided a cost-effective and ultrasensitive technique for spike RBD detection. The key element of this system was a disposable conducting nanocomposite consisting of Epoxy functional group-substituted thiophene monomer (*EpoxyS-Thi*)- and acetylene black (AB)-modified indium tin oxide (ITO) electrodes. The utilized interface material *EpoxyS-Thi* was synthesized and electrodeposited on the single-use ITO platform in the presence of AB by employing a cyclic voltammetry technique, for the first time. The fabricated biosensor had excellent selectivity for spike RBD protein, and the capability of such a sensor system to selectively recognize the target RBD protein was studied through electrochemical impedance spectroscopy (EIS) in the presence of a redox pair.

Conjugated polymers (CPs) have attracted considerable interest in view of their unique electrochemical features such as good conductivity, ease of preparation, and suitable environmental stability with their precious optical and electrical features as well as suitable mechanical characterizations; they have been used as an interesting working area in electrochemical biosensing technology.[21,22] The possibility of utilizing CPs as an appropriate biosensing interface for biological molecule attachment makes them remarkable candidates for biosensing system fabrication.[23,24] CPs provide a compatible microenvironment for biomolecules, and therefore, they are preferred as an immobilization platform for immobilization of antibodies, enzymes, DNA, and receptors.[25] CPs such as polypyrrole, polyaniline, and polythiophene have been extensively employed for biosensor construction.[26] Polythiophene is one of the most utilized CPs. Owing to its good biocompatibility, simple synthesis, high stability, and good mechanical properties, polythiophene is one of the most significant π-CPs with potential applications in sensors, electrochromic devices, thermal conductors, and thermo electric apparatuses.[27,28] For the preparation of polythiophene polymeric thin films, chemical oxidation, electrochemical oxidation, and oxidative chemical vapor deposition techniques have been utilized.[29] Nowadays, the most popular approach to polymerize thiophene monomers is electrochemical oxidation polymerization because the controlling of the polymerization degree is easy.[30] Electrochemical polymerization of the monomer as a film has ensured a strong and easy way to realize film layers with controlled thickness, electrical conductivity, and ion transport.[31,32] Electrodeposition is a fast and effective technique for deposition of particles from the electrolyte onto the working platform surface in situ employing appropriate voltages. The doping and polymerization of particles and a monomer can be performed at the same time employing electrodeposition, without the requirement for reductants or oxidants. In addition, the thickness and features of functionalized surfaces can be checked by using the electrochemical parameters.[33]

AB is one of the carbonaceous materials, and it is produced by the controlled combustion of acetylene in air under pressure. Thanks to its spongy structure and numerous attractive features such as high electrical conductivity, huge surface area, low cost, and robust adsorptive capability. AB has gained interest of researchers, and it has been usually utilized in electrochemical applications.[34] Nevertheless, the construction of biosensors by integrating an *EpoxyS-Thi* polymer and AB composite (conducting nanocomposite, *C-NC*) for biosensor fabrication has not been noticed in the literature. In recent studies, it has been utilized as a substitute of graphitic powder in production of carbon paste electrodes, mixed with a chitosan material to functionalize a glassy carbon electrode (GCE), and dispersed in water in the presence of dihexadecyl hydrogen phosphate to form a film onto the GCE.[35,36] The *C-NC* film had outstanding features such as good electrical conductivity and large specific surface area, and these properties made it an ideal biosensing interface for antibodies.

In this work, *EpoxyS-Thi* and AB were employed to form a *C-NC* layer by using an electrodeposition process. The *P*(*EpoxyS-Thi*) polymer supplied active epoxy functional groups, which could provide immobilization of target analyte specific antibodies. AB is a carbonaceous material and enhances the electron transfer. The electrodeposition of AB and *EpoxyS-Thi* caused a homogenous *C-NC* layer with epoxy groups, large specific surface area, and satisfactory conductivity. Here, a novel strategy for construction of a *C-NC* layer was fabricated by electrodeposition of AB particles incorporating polymerization of an *EpoxyS-Thi* monomer onto an ITO electrode, for the first time. By using this technique, a label-free immunosensing system based on a new *C-NC* layer was successfully manufactured and applied to detect the RBD antigen in artificial nasal secretion samples. The *C-NC* layer-modified electrode had dual functions; the *EpoxyS-Thi* polymer accelerated the electron transport and enhanced the sensitivity of the proposed biosensor. Moreover, the produced polymer provided suitable binding sites for antibodies, which was specific to the target antigens. The thickness of the *C-NC* layer could be checked by employing the electrodeposition method, a diverse superiority over previously utilized technique. The

https://doi.org/10.1021/acsbiomaterials.1c00580
ACS Biomater. Sci. Eng. 2021, 7, 3874−3885

Scheme 1. *C-NC*-deposited electrode preparation and the RBD biosensor

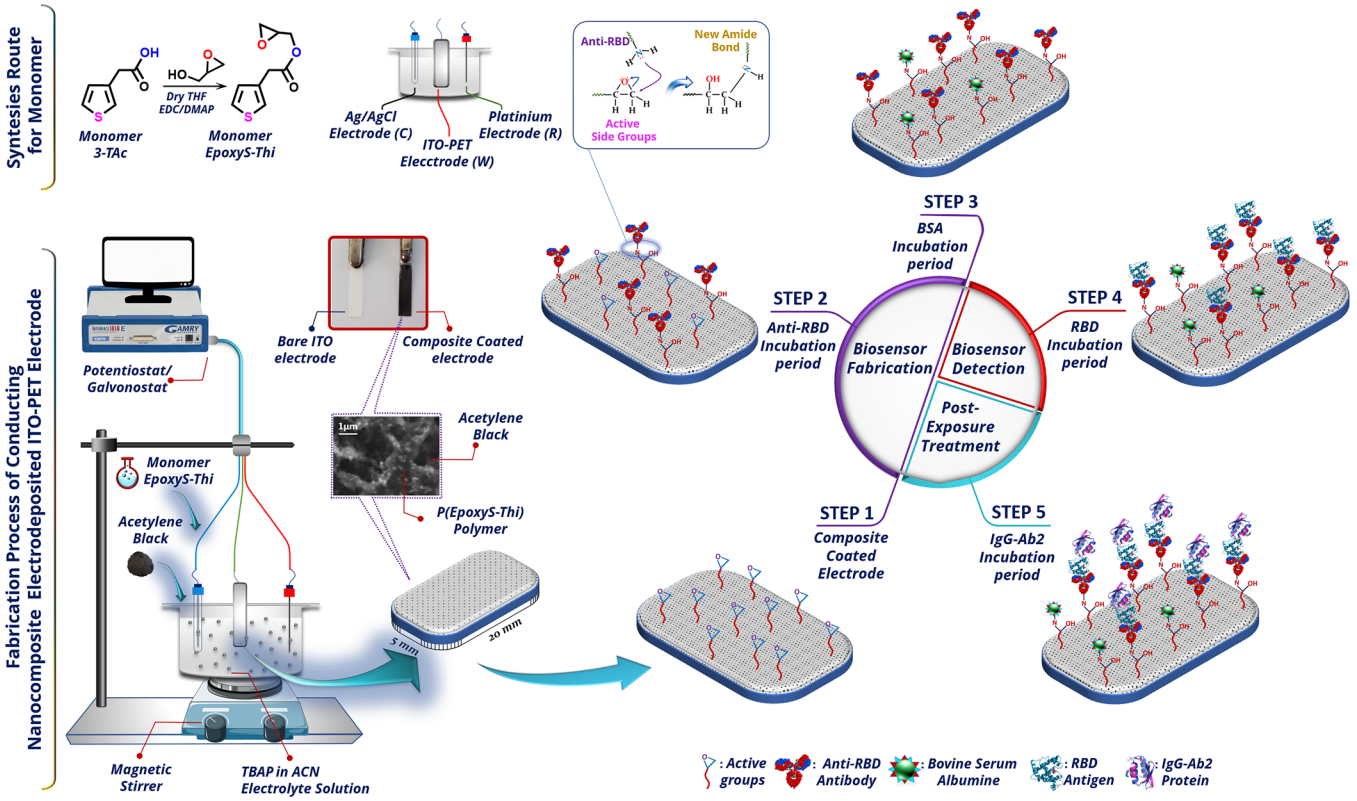

electrodeposition of AB particles and electropolymerization of *EpoxyS-Thi* were examined by EIS and cyclic voltammetry (CV) techniques. The surface morphology of the functionalized electrode was studied by scanning electron microscopy (SEM). The selectivity of the biosensor toward other protein molecules was investigated. The developed probable and versatile impedance biosensing strategy showed excellent performance for detection of RBD molecules.

2. EXPERIMENTAL SECTION

All utilized materials and reagents in RBD biosensor fabrication and devices utilized for characterization of the RBD biosensor are available in the Supplementary Material File.

2.1. Preparation of the Epoxy Thiophene Monomer. The epoxy thiophene monomer (*EpoxyS-Thi*) was synthesized from the simple esterification reaction between 3-thienylacetic acid (3-Tac) and glycidol (Gly) at 35 °C under an argon gas by modifying the procedures found in the literature.[23,37,38] Column chromatography was used for monomer purification. (Colorless liquid, 70%, yield). FTIR(ATR) cm^{-1}: 3100; 3057; 2927; 3001; 2880; 1735(C═O); 1537; 1481; 1411; 1257; 1132; 1082; 1009; 907; 857; 760; 733; 700; 612 (Figure SI-2). Raman ($\lambda_{laser\ =\ 780\ nm}$): 3110; 2996; 2934; 1738 (C═O); 1541; 1413; 1259; 1153; 1084; 994; 947; 925; 861; 837; 677; 615 (Figure SI-3). Proton-NMR ($CDCl_3$): 7.30 ppm (Ha), 7.06 ppm (Hb), 7.18 ppm (Hc), 3.72 ppm (Hd), 4.45 and 3.98 ppm (He), 3.22 ppm (Hf) and 2.84 and 2.62 ppm (Hg) (Figure SI-4).

2.2. Preparation of the *C-NC*-Electrodeposited Electrode and Sensing System Fabrication. Prior to modification, ITO was subjected to cleaning with acetone, soap solution, and ultrapure water in an ultrasonic bath and rinsed thoroughly with ultrapure water. After the cleaning operation, 100 mg of AB and the *EpoxyS-Thi* monomer (0.1 mg/mL) were added in electrolyte solution (tetrabutylammonium perchlorate (TBAP) in acetonitrile 0.1 M), and the clean electrode was modified applying potential 5 cycles between +0.2 V and 2.0 V with a 100 mV/s scan rate. After modification, the *C-NC*-modified electrode was rinsed thoroughly with acetonitrile and ultrapure water. The rinsed electrode was used for the next step. Anti-RBD antibodies were attached on the *C-NC*-coated electrode surface by immersing the ITO/*C-NC* in a solution of anti-RBD antibodies (5 ng/mL) for 1 h. Active epoxy groups of the *C-NC* composite linked to amino groups of anti-RBD via the ring opening reaction. After rinsing the antibody-immobilized electrode surface with ultrapure water, they were incubated in BSA solution (0.5%) for 1 h to deactivate the remaining epoxy groups present on the electrode surface. In this way, one can ensure that the RBD antibodies were immobilized only to the epoxy groups present on the electrode surface. The anti-RBD antibody-immobilized electrode surface could be utilized immediately as an immunosensor or kept dry at 4 °C for a long time without any reduction in the sensitivity. For RBD determination, the modified electrodes were incubated in RBD antigen solution for 45 min. The developed immunosensor was washed with ultrapure water prior to electrochemical analysis. Finally, goat antirabbit IgG secondary antibody (Ab_2, 250 pg/mL) was immobilized on the sensing system to amplify the signal of the sandwich-type electrochemical immunosensor.

2.3. Impedimetric Determination Procedure. In the impedance-based immunosensor, the determination of a target is based on the principle that any molecule immobilized on the electrode surface will alter the recorded impedance.[39] In this instance, the specific binding between the anti-RBD antibody and RBD antigen forms a coating film, which affects the impedimetric signal.

Impedance analyses were performed at a DC voltage of 0 V and an AC voltage of 5 mV. The impedance spectra was taken in 5 mM $[Fe(CN)_6]^{3-/4-}$ and 1 M KCl within the frequency range from 0.5 Hz to 50 kHz. The impedance spectra were fitted to the Randle's equivalent circuit with Gamry Analyst software. To determine the RBD concentration, EIS of the biosensor (ITO/*C-NC*/anti-RBD/BSA) was first performed without RBD antigen addition. Following the measurement, the biosensor was immersed in RBD solution and incubated for 60 min under ambient conditions to allow the antigen attachment to the RBD specific antibodies. After this, the electrode surface was washed with ultrapure water and dried under argon gas. In

https://doi.org/10.1021/acsbiomaterials.1c00580
ACS Biomater. Sci. Eng. 2021, 7, 3874−3885

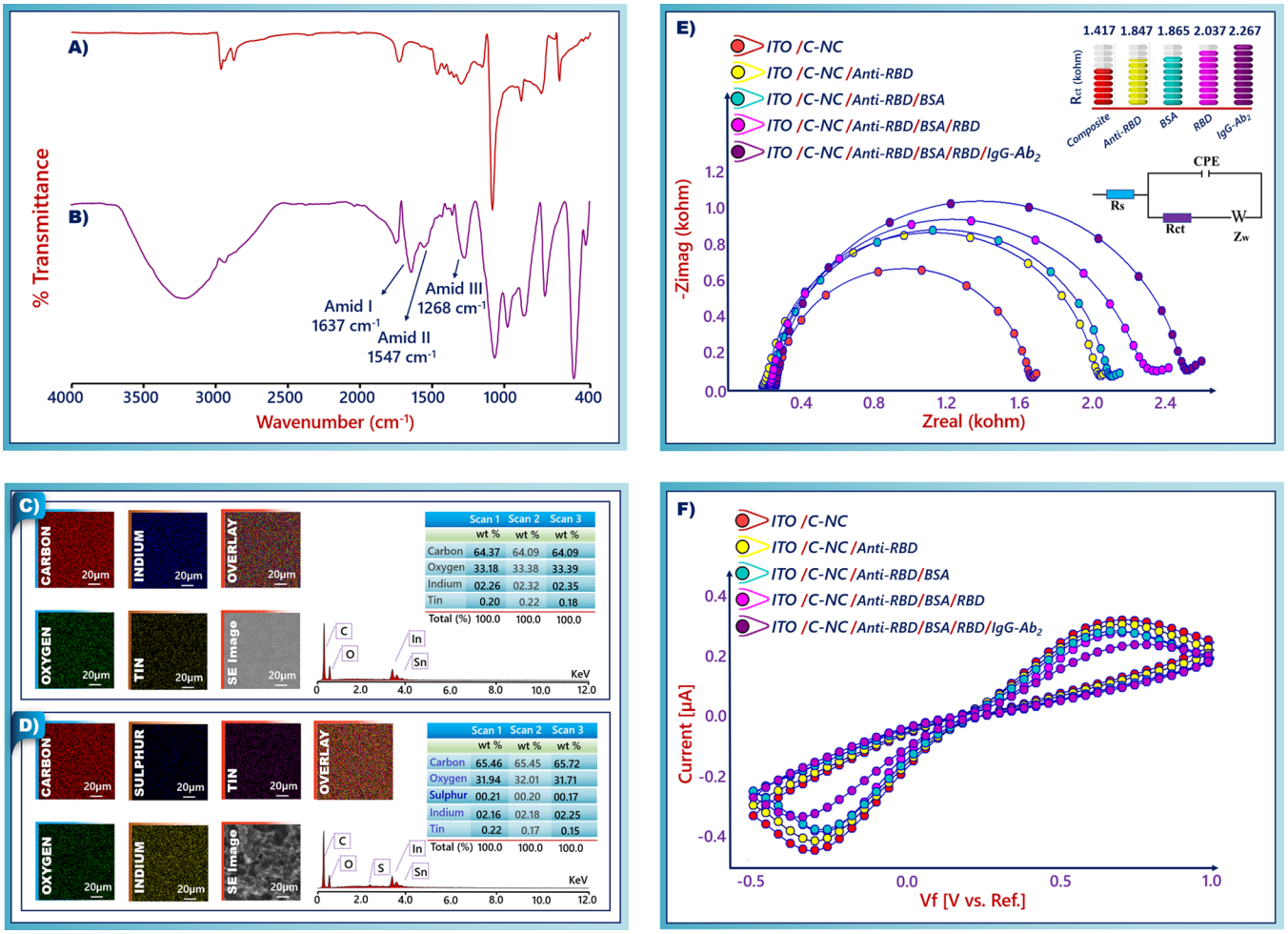

Figure 1. FTIR spectra of (A) ITO/*C-NC*, (B) ITO/*C-NC*/anti-RBD; (C) EDX of bare ITO, (D) ITO/*C-NC*; (E) EIS and (F) CVs after biosensor fabrication steps.

the last step of the biosensor fabrication, ITO/*C-NC*/anti-RBD/BSA/RBD was incubated in Ab_2 solution for 1 h to increase the signal of the biosensing system and to obtain a more sensitive immunosensor. Finally, the EIS signal of ITO/*C-NC*/anti-RBD/BSA/RBD/Ab_2 was measured.

2.4. Analysis of Nasal Secretions. Nasal secretions are derived chiefly from submucosal glands and goblet cells. SARS-CoV-2 spike RBD can be detected in nasal and oral cavities. Therefore, nasal secretions were chosen an appropriate analysis matrix for coronavirus. Nasal secretion includes water (95%), glycoproteins (2%) such as albumin, immunoglobulins, lysozyme, lactoferrin, and others, inorganic salts (1%), and lipids (<1%).[40] In order to test the produced immunosensor in analytical application, artificial nasal secretion samples were prepared by using water, immunoglobulin G, immunoglobulin H, and inorganic salts. Five different concentrations of RBD were added to these solutions, and the determinations of added RBD concentrations were performed 3 times.

3. RESULTS AND DISCUSSION

The spike RBD biosensor was prepared in a five-step procedure. First, the one-step synthesis of a *C-NC* layer consisting of an *EpoxyS-Thi* monomer and AB was constructed on the cost-effective ITO substrate. This *C-NC* deposition onto the ITO electrode surface was a crucial step for obtaining a successful biosensor with improved performance (Step 1). After a homogeneous layer formation on the electrode, spike RBD specific antibodies were immobilized on the *C-NC*-covered surface (Step 2). The prepared ITO was modified by incubating in BSA solution to deactivate the active ends (Step 3); then, the anti-RBD connected specifically to their target RBD protein (Step 4). Finally, the resulted electrode was exposed to Ab_2 (Step 5).

3.1. Chemical Characterizations of Fabricated Electrodes. Synthesis of the epoxy thiophene monomer (*EpoxyS-Thi*) was successfully carried out with the Steglich esterification reaction. This simple and easy reaction method is displayed in Scheme 1. The chemical features of the monomer were examined with various spectral methods (Fourier-transform infrared spectroscopy (FTIR), DXR-RAMAN, and proton nuclear magnetic resonance) to prove the successful synthesis of the thiophene monomer, and analysis results are given in detail in the Supporting Information File. The chemical composition and surface features of the *C-NC*-covered ITO substrate and anti-RBD-immobilized ITO surface were characterized via FTIR spectroscopy (Figure 1). The FTIR spectra of *C-NC*-deposited ITO (A) and anti-RBD antibody-immobilized ITO (B) surfaces are shown in Figure 1, respectively. As illustrated in Figure 1A, specific absorption peaks of the epoxy group in the *C-NC* were observed at 876 and 926 cm^{-1}, which were derived from the C−O deformation and C−O−C of the epoxy functional group, respectively.[41] The peak at 2927 cm^{-1} can be assigned to the C−H stretching.[42] The strong peak at 1726 cm^{-1} was referred to the carbonyl group (C═O) in the repeating unit of the

https://doi.org/10.1021/acsbiomaterials.1c00580
ACS Biomater. Sci. Eng. 2021, 7, 3874−3885

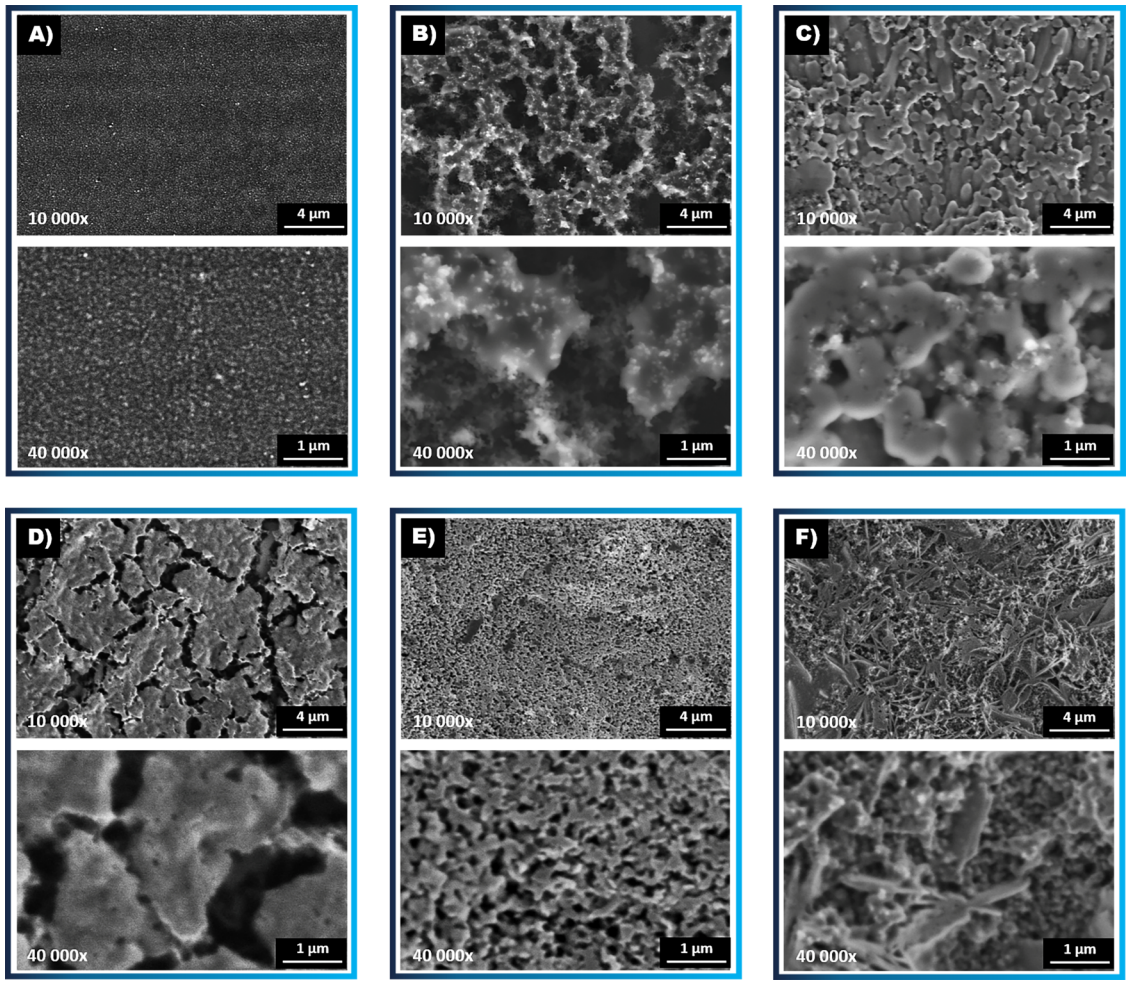

Figure 2. SEM images of the (A) bare electrode surface, (B) *C-NC*-deposited electrode surface, and (C) anti-RBD antibody, (D) BSA, (E) RBD antigen, and (F) Ab_2 immobilized electrode surface.

polymer.[43,44] FTIR spectroscopy is a well-known analytical method to characterize the samples with biological origins. Many biomolecules (proteins, lipids, nucleic acids, and carbohydrates) have characteristic and specific vibrational peaks, which can be observed by using FTIR analysis. The amide *I* (C═O stretching, 1600−1700 cm^{-1}), amide II (N−H bending, 1500−1600 cm^{-1}), and amide III (C−N stretching and N−H bending, 1200−1330 cm^{-1}) are known as different predominant FTIR bands in biological samples.[45] When FTIR spectra of Figure 1A,B were examined, the peak variations in spectra were completely different. Amide *I* (1637 cm^{-1}), amide II (1547 cm^{-1}), and amide III (1268 cm^{-1}) peaks were seen as broad and intense bands in the spectrum of the anti-RBD antibody-immobilized electrode surface, respectively (Figure 1B). These characteristic bands of biological molecules obviously proved the existence of the anti-RBD immobilization.

Addition to FTIR measurements, energy-dispersive X-ray spectroscopy (EDX) analyses were utilized to confirm the successful *C-NC* layer formation. Figure 1C,D displays the electrode surface before and after *C-NC* layer formation. As seen in these figures, after *C-NC* layer coating, the sulfur (S) atom was fixed on the working electrode. The S atom was found in the structure of the *EpoxyS-Thi* monomer, and the presence of this atom verified the efficient electrodeposition on the working electrode. In addition, the S proportions fixed on the electrode surface were measured in three different regions. The as-prepared electrodes included similar S proportions, and this situation confirmed the homogenous *C-NC* layer formation.

3.2. Electrochemical Characterizations of RBD Biosensor Fabrication Steps. EIS and CV analyses were performed to characterize the interface features of the functionalized electrodes during the immunosensor generation. EIS was an efficient system for working electrode surface investigation. The proper binding of each biomolecule was confirmed through EIS analyses.[46,47] In every situation, Nyquist diagrams of the modified electrodes possess a semicircle part and a linear part. The semicircle at higher frequencies and a linear at lower frequencies are associated with the electron transfer and diffusion processes, respectively. The semicircle diameter means the electron transfer resistance (R_{ct}).[48] The impedance of a biosensing system is fitted to classical Randle's equivalent circuit, which has ohmic resistance of the electrolyte (R_s), constant phase element, Warburg impedance (W), and electron transfer resistance (R_{ct}) (Figure 1E inset).

Figure 1E illustrates the Nyquist diagrams of impedance spectra recorded after different modification steps. In addition, EIS gave information about barrier features of the layer variations in the modification procedures. As can be seen from Figure 1E, *C-NC*-modified ITO had a very small semicircle

https://doi.org/10.1021/acsbiomaterials.1c00580
ACS Biomater. Sci. Eng. 2021, 7, 3874−3885

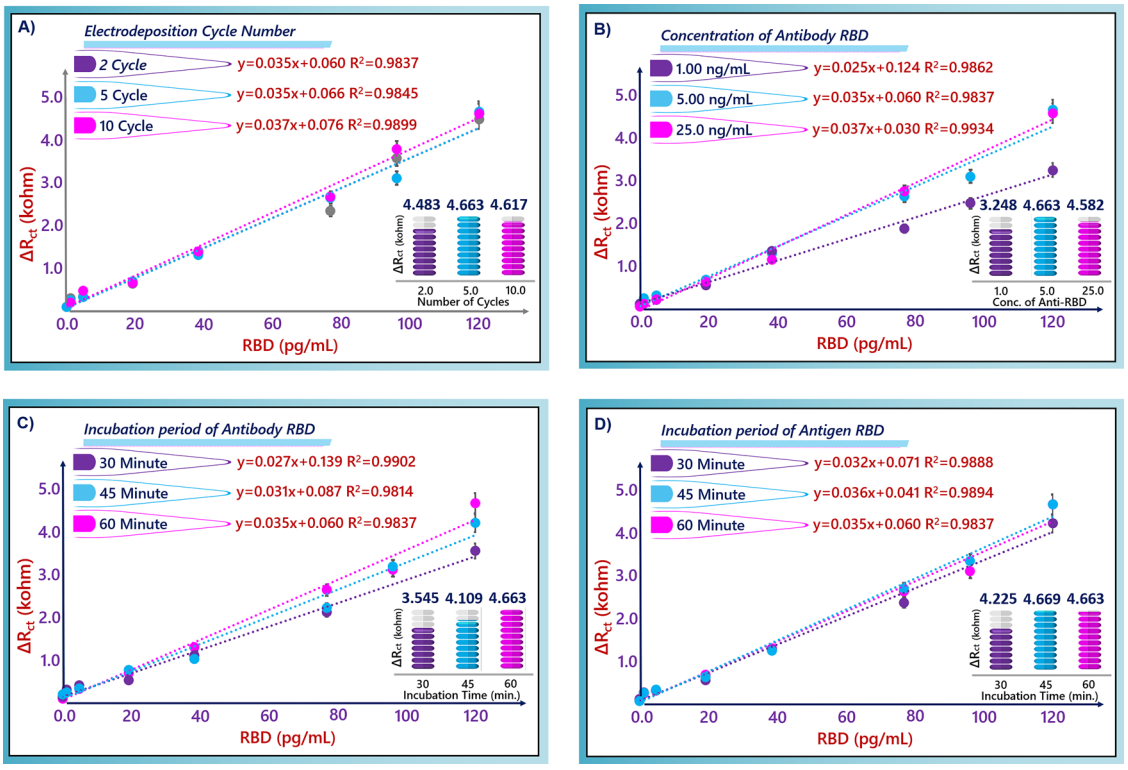

Figure 3. Relationship between immunosensor signals and concentrations of (A) *C-NC*, (B) anti-RBD, (C) anti-RBD incubation time, and (D) RBD incubation time.

diameter, indicating a very low electron transfer resistance. After the immobilization of the anti-RBD on the ITO sheet surface, an increment in the semicircle diameter was seen due to the formation of a nonconductive protein coating. Afterward, the R_{ct} value increased when BSA molecules blocked free epoxy ends present on the electrode surface. At the last step, (detection step), the R_{ct} increased when the ITO/*C-NC*/anti-RBD/BSA was utilized to determine the RBD antigen; the RBD antigen coupled to anti-RBD antibodies present on the electrode surface offered a nonconductive layer. In the postexposure step, an anti-Ig G protein (Ab_2, 250 pg/mL) molecule was utilized to increase the immunosensor signal and a protein coating was constructed on the functionalized ITO surface after Ab_2 immobilization. Because of this reason, an increment was seen in the R_{ct} value of the system and the electrode surface became more insulating. Table SI-1 summarizes the R_{ct} values of the fitting EIS signals for the biosensor development steps.

Furthermore, CV was utilized to characterize the changes formed on the modified electrode surface after each immobilization step (Figure 1F). As seen from Figure 2B, the *C-NC*-electrodeposited electrode displayed high peak currents due to the conductive feature of AB. After immobilization of anti-RBD antibodies, the peak currents were decreased due to generation of a barrier effect from protein molecules. Moreover, BSA blockage caused decreases in peak currents. After the target RBD antigen recognition by the attached anti-RBD antibody, decreases were observed in peak currents, illustrating that the electron transfer kinetics of the redox couple were prevented. Finally, with the treatment with Ab_2 protein on the electrode surface, decreases were seen in peak currents in view of the insulating character of Ab_2.

3.3. Surface Imaging by SEM. SEM analysis was employed for characterization of the electrode surface imaging after each modification stage. Figure 2A shows the bare ITO surface observed with SEM, and a homogenous clean appearance was obtained. This appearance is the characteristic feature of the ITO sheet. As seen in Figure 2B, *C-NC* electrodeposited nicely onto the bare electrode surface and AB dispersed uniformly on the ITO working electrode. Additionally, the *EpoxyS-Thi* polymer film was coated on the electrode surface and a homogeneous structure was observed. Thus, a suitable surface was formed for anti-RBD antibody immobilization. After anti-RBD antibody immobilization, the noticeable change in morphology was observed due to well-immobilized antibody molecules (Figure 2C). The blockage of epoxy ends with BSA molecules, causing changes on the electrode surface (Figure 2D). The RBD antigen was bound to antibodies specifically and changed the electrode surface morphology (Figure 2E). A clustered dense surface was observed after immobilization of Ab_2 protein on the electrode surface (Figure 2F). Thus, it can be clearly seen that the morphological feature of the electrode surface was changed after different fabrication steps, referring polymer deposition, biorecognition element immobilization, and target analyte coupling.

3.4. Optimization of Experimental Parameters. In order to form a *C-NC* layer on the electrode surface, the *EpoxyS-Thi* monomer and AB were added in TBAP (0.1 M). *EpoxyS-Thi* was the basic material in the biosensor construction procedure because it offered attachment points for biorecognition element immobilization. That is why, it was very essential to optimize the amount of *EpoxyS-Thi* to generate a *C-NC* layer, which was developed for ultra-sensitive and highly stable impedimetric immunosensors. This layer had

https://doi.org/10.1021/acsbiomaterials.1c00580
ACS Biomater. Sci. Eng. 2021, 7, 3874−3885

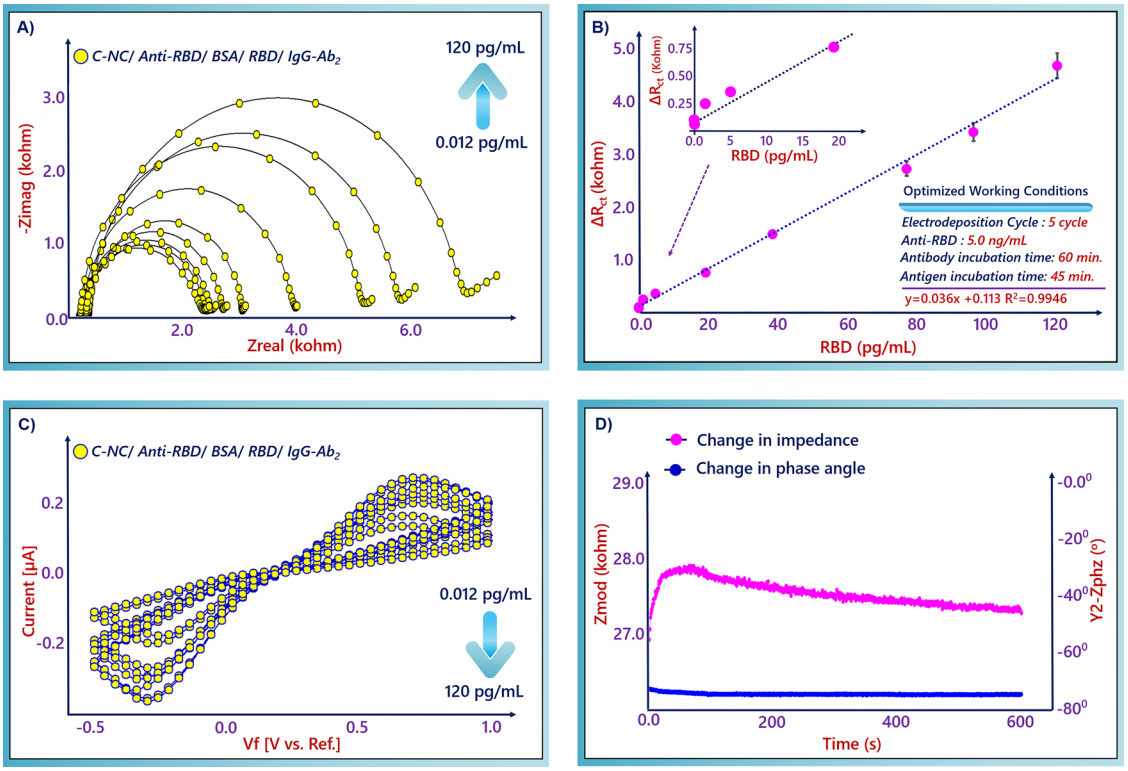

Figure 4. (A) Typical EIS spectra and (C) CVs corresponding to the biosensor incubated in different RBD concentrations. (B) Calibration curve and (D) SFI result for the RBD biosensor.

advantages such as high electrical conductivity, suitable biocompatibility, and covalent linking capability. The formed *C-NC* layer provided a high concentration of epoxy groups, which were attachment points of antibodies. The quality of the *C-NC* layer was influenced by electropolymerization duration, and the feature of the polymer depended on layer thickness and electrodeposition. In order to obtain optimum thickness, *EpoxyS-Thi* monomers and AB were deposited on the ITO electrode with scans between 2 and 10 cycles. Different scan cycles were applied to fabricate a suitable biosensing matrix material for attachment of biorecognition elements. As observed in Figure 3A, the highest immunosensing signal was measured after 5-cycle electrodeposition. If the *C-NC* layer is too dense, diffusion difficulties between the electrode surface and biological molecules may form, and a low electron transfer rate can be achieved. Conversely, if the *C-NC* layer is too thin, enough biological molecules do not attach on the electrode surface. Therefore, the immunosensor prepared with 5-cycle electrodeposition had a high signal and a good immobilization structure. Because of this, 5-cycle electrodeposition was used for subsequent experiments.

In order to achieve the best immunosensing response of a biosensor, the utilized biorecognition element amount is another important parameter. In the range of 1−25 ng/mL anti-RBD concentration, impedimetric signals were recorded. Figure 3B shows that the maximum impedimetric signal was acquired at the 5 ng/mL anti-RBD antibody level. The usage of low levels of anti-RBD antibody caused low response, and the increase in anti-RBD concentration did not increase the impedimetric signal. As a result, 5 ng/mL was used as the optimum level for development of the proposed immunosensor.

The incubation duration is another effective parameter on the analytical response of the suggested immunosensor. Thus, incubation times of anti-RBD and RBD proteins were optimized. For optimization of anti-RBD antibody incubation time, experiments were performed with different incubation periods from 30 to 60 min. As displayed in Figure 3C, the biosensor reached the maximum response at 60 min. Therefore, a 60 min incubation period was selected as the optimum binding time, and this duration was utilized in further experiments. For optimization of RBD antigen incubation time, three different times (30, 45, and 60 min) were employed. As illustrated in Figure 3D, the electrochemical signals were close to each other after 45- and 60-min incubation. Consequently, 45 min was applied in the following experiments.

3.5. Analytical Characteristics of the Designed RBD Immunosensor. The analytical determination ability of the designed immunosensor was studied under optimal experiment conditions. Different concentrations of RBD antigen were determined by the EIS technique employing the *C-NC*-functionalized ITO electrode. The electrochemical analyses were performed after the RBD antigen binding on the anti-RBD-immobilized ITO electrode. The ITO/*C-NC*/anti-RBD/BSA electrodes were immersed in various concentrations of RBD solutions (0.0012−120 ng/mL) and incubated for 45 min. The specific immunointeraction between the anti-RBD antibody and RBD antigen prevented the electron transfer and increased impedimetric signal. Figure 4A illustrates the Nyquist plots of the developed biosensor, and the fitting R_{ct} values are represented in Table SI-1B. The impedimetric results displayed that the Nyquist diagram semicircle diameter increased with the increasing RBD antigen concentration because more antigen biomolecules were bound to immobilized anti-RBD

https://doi.org/10.1021/acsbiomaterials.1c00580
ACS Biomater. Sci. Eng. 2021, 7, 3874−3885

Table 1. Comparison of RBD Sensing Systems

sensing system	sensing type	detection range (pg/mL)	detection limit (pg/mL)	ref
1-pyrene butyric acid N-hydroxysuccinimide ester-modified SPE	electrochemical	20×10^6-80×10^6	20×10^6	20
cofunctionalized TiO_2 nanotubes	electrochemical	0.721−72.1	36	17
anti-S1 cell-based biosensor	colorimetric	10^{-2}−10^6	1	19
paper-based ePAD	colorimetric	10^3−10^6	11×10^5	11
lateral flow assay	colorimetric	5×10^3-5×10^5	10^6	18
C-NC-modified ITO	electrochemical	0.0012−120	0.00058	present study

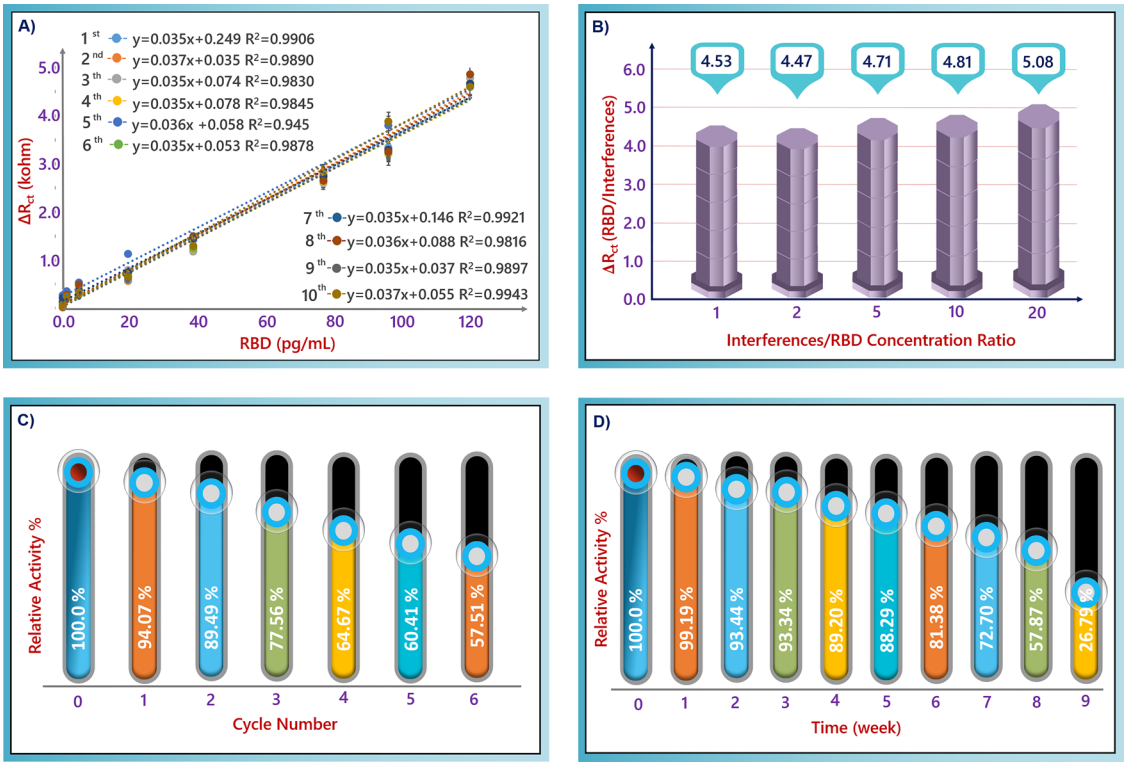

Figure 5. (A) Reproducibility study, (B) selectivity study of the ITO/*C-NC*/anti-RBD/BSA electrode in the presence of different interferents, (C) reusability, and (D) storage stability of the RBD biosensor.

antibodies. Thus, the electron transfer was prevented and resulted in the increase of R_{ct} values. Similarly, the peak currents (Figure 4B) were decreased with the increasing RBD antigen concentration. A linear curve was drawn for the impedimetric signal in relation to the RBD antigen level. Figure 4C illustrates the calibration graph of RBD, and as observed from Figure 4C, the ΔR_{ct} of modified surfaces increased with the increase in RBD concentrations. A wide linear detection range was determined in the range from 0.0012 to 120 pg/mL with a limit of detection of 0.58 fg/mL (S/N = 3) using this label-free immunosensor. The linear equation of the calibration curve was $\Delta R_{ct}(k\Omega) = 0.036$ [RBD] + 0.113, and the sensitivity was calculated to be 0.15 kohm $pg^{-1}mL\ cm^{-2}$. These results illustrated that the developed biosensor was more sensitive than the other previously developed impedimetric biosensors, in this instance of the limit of detection and linear detection range for RBD analysis (Table 1). Vadlamani et al. (2020) developed a Co-TNT)-based electrochemical sensing system for rapid detection of the spike RBD present on the virus surface. In order to construct to this system, a one-step electrochemical anodization route was used for synthesizing TNTs and an incipient wetting method for cobalt functionalization of the TNT platform.[17] The fabrication process of this system was more expensive and longer than our proposed sytem, and it had a higher LOD compared to the proposed system. Lee et al. (2021) fabricated an LFA-based system for detection of SARS-CoV-2 spike 1 (S1) protein using the SARS-CoV-2 receptor ACE2.[18] This system was usable, but it requried viral RNA purification and RT-qPCR before the analysis. The proposed *C-NC*-based system had a simple and facile production procedure compared to this LFA-based system. An anti-S1 cell-based biosensor was developed based on membrane-engineered mammalian cells bearing the human chimeric spike S1 antibody for detection of spike protein, and this system required membrane engineering and cell culture production.[19] This sytem was different, but specialized personnel was required for development of this system. An electrochemical immunosensor based on 1-pyrene butyric acid N-hydroxysuccinimide ester-modified screen-printed electrode (SPE) was developed for spike protein detection by using a square wave voltammetry technique.[20] The developed biosensor had a higher LOD and narrower detection range than our proposed immunosensor. It can be observed that the analytical performance of the developed biosensor was suitable for analysis of spike RBD protein detection due to its distinct properties.

https://doi.org/10.1021/acsbiomaterials.1c00580
ACS Biomater. Sci. Eng. 2021, 7, 3874−3885

For in situ monitoring of specific interaction between anti-RBD and RBD, single frequency EIS (SFI) was used to measure the antigen binding time profile. In single frequency EIS analysis, the impedance was measured at constant frequency.[49] The ITO/*C-NC*/anti-RBD/BSA electrode was the working electrode, and it was immersed in the conventional three-electrode system containing RBD solution (19.2 pg/mL). The impedance versus time plot was recorded. As seen in Figure 4D, the RBD antigens were captured by antibodies immobilized on the *C-NC*-deposited electrode, and an increase in impedance was determined.

3.6. Repeatability, Reproducibility, Long-Time Stability, Selectivity, and Reusability of the RBD Immunosensor. For the application in the clinical diagnosis, repeatability, reproducibility, long-term stability, selectivity, and regeneration of the biosensing tool are very important. The repeatability of the biosensor was examined by employing 20 identical modified electrodes (ITO/*C-NC*/anti-RBD/BSA) and the prepared electrodes used for measurement of RBD antigen (32 pg/mL). A relative standard deviation (RSD) was calculated to be 5.74%, illustrating appropriate repeatability of the biosensor (Figure SI-5). The reproducibility test was performed by using 10 immunosensors independently fabricated in the identical experimental situations. The RSD was calculated to be 2.24%, illustrating good reproducibility of the immunosensing system (Figure 5A).

The selectivity of the immunosensor for detecting RBD was studied by using nucleocapsid protein and other biological markers found in nasal secretions (interleukin 8, interleukin 1β, and tumor necrosis factor α).[50] In this experiment, the ratios of the utilized interferent concentration to the concentration of RBD antigen were 1:1(96 pg/mL: 96 pg/mL), 2:1 (192 pg/mL: 96 pg/mL), 5:1(480 pg/mL: 96 pg/mL), 10:1 (960 pg/mL: 96 pg/mL), and 20:1 (1920 pg/mL: 96 pg/mL). Figure 5B represents that these biological markers did not immunoconjugate with anti-RBD, and thus, they did not interfere in the detection of RBD. The high selectivity of this immunosensor was originated from the bioimmuno response of a successful biosensor construction procedure.

The regeneration capability of the impedimetric immunosensor is critically significant for biosensing applications. The fabricated immunosensor was regenerated after dipping the prepared working electrode in the acidic solution. The RBD antigen-immobilized electrode was regenerated in HCl (0.1%) solution reutilized for measurement of RBD antigen. The immunosensor displayed reusability until the 5th acid treatment retaining 60.41% of the impedimetric signal (Figure 5C).

The long-time stability of the biosensing platform was also studied because this parameter was a significant factor for the practical application of the immunosensor. When the electrodes were in use, they were stored at 4 °C. The activity of the electrodes was measured at intervals of 7 days for the detection of RBD antigen (38.4 pg/mL). The developed immunosensor could retain its EIS signal (72.70%) after 7 weeks storage duration at 4 °C. This result illustrated that the designed immunosensor had proper stability for RBD detection. This good long-time stability result may be obtained owing to the covalent binding between epoxy groups of *EpoxyS-Thi* and amino groups of anti-RBD, which could prevent the breaking out the antibodies (Figure 5D).

3.7. Applications of the RBD Immunosensor to Nasal Secretions. The possibility of the suggested immunosensor for potential clinical analysis was investigated using artificial nasal secretions and nasal secretions obtained from healthy volunteers. First, artificial nasal secretions were prepared by using water, immunoglobulin G, immunoglobulin H, and inorganic salts. Five different concentrations of RBD were added to artificial nasal secretions and nasal secretions obtained from healthy volunteers' solutions, and the ITO/*C-NC*/anti-RBD/BSA electrodes were used for determinations. The determinations of RBD concentrations were performed 3 times. The obtained recovery rates of this analysis illustrated that the suggested method was suitable for detection of RBD antigen with low concentrations. As summarized in Tables 2 and 3 the recovery rates were found to be 97.16−107.23 and 87.44−104.97% for artificial nasal secretions and nasal secretions obtained from healthy volunteers, respectively, which clearly indicated the potentiality of the proposed immunosensor for the analytical application in nasal secretions.

Table 2. Results of Artificial Nasal Secretions

sample	added RBD (pg/mL)	found using the biosensor (pg/mL)	SD[a] and CV[a] (%)	recovery (%)	relative difference (%)
1	0.10	0.10	2.02−14.42	100.05	0.05
1	0.10	0.10		100.05	0.05
1	0.10	0.13		100.90	0.90
2	1.20	1.40	0.11−7.89	104.67	4.67
2	1.20	1.29		102.12	2.12
2	1.20	1.51		107.23	7.23
3	19.20	18.81	0.25−1.32	98.28	−1.72
3	19.20	18.57		97.16	−2.84
3	19.20	19.06		99.39	−0.61
4	38.40	38.91	0.81−2.05	101.23	1.23
4	38.40	38.94		101.30	1.30
4	38.40	40.32		104.63	4.63
5	96.00	95.91	1.09−1.14	99.91	−0.09
5	96.00	96.30		100.30	0.30
5	96.00	94.25		98.23	−1.77

[a]SD, standard deviation; CV, coefficient variation.

Table 3. Nasal Secretions Obtained from Healthy Volunteers Using the Suggested RBD Biosensor

sample	added RBD (pg/mL)	found with the biosensor (pg/mL)	SD[a] and CV[a] (%)	recovery (%)	relative difference (%)
1	1.20	1.02	0.15−15.61	95.74	−4.26
1	1.20	0.82		91.27	−8.73
1	1.20	1.13		98.29	−1.71
2	1.20	1.21	0.10−7.42	100.21	0.21
2	1.20	1.32		102.76	2.76
2	1.20	1.40		104.67	4.67
1	38.40	33.18	0.96−2.83	87.44	−12.56
1	38.40	33.38		87.90	−12.10
1	38.40	34.93		91.64	−8.36
2	38.40	36.01	2.26−5.88	94.24	−5.76
2	38.40	38.91		101.23	1.23
2	38.40	40.46		104.97	4.97

[a]SD, standard deviation; CV, coefficient variation.

Lescure et al. (2020) reported that the virus load in nasopharyngeal swabs from two COVID-19 positive patients

https://doi.org/10.1021/acsbiomaterials.1c00580
ACS Biomater. Sci. Eng. 2021, 7, 3874−3885

6.25 × 10^5 and 3.0 × 107 PFU/mL.[51] The Simoa assay illustrated that the signal from 1700 PFU of recombinant SARS-CoV-2 correlates with the signal from about 1 pg of pure Spike antigen.[19] In this case, the developed immunosensor could determine Spike RBD protein at a concentration of 0.0012 pg/mL, while the lowest significant signal from SARS-CoV-2 was detected from 33 × 10^{-2} PFU/mL. This correlates with 16.5 × 10^{-4} PFU of recombinant SARS-CoV-2 per pg of pure Spike antigen.

4. CONCLUSIONS

In this study, an ultra-sensitive and highly specific impedimetric immunosensing system based on a *C-NC* layer-modified ITO electrode was manufactured to determine RBD antigen, and it was successfully utilized in the analysis of nasal secretions. The *C-NC* was fabricated by the electrodeposition process and provided proper epoxy groups to the electrode surface, which was necessary for biomolecule immobilization. The *C-NC* increased the conductivity of the electrode surface because of the high conductivity of AB. This composite enhanced the sensitivity of the electrode by accelerating the electron transfer rate and increment in the number of antibodies linking points for anti-RBD attachment. Furthermore, this composite maintained the immunoactivity of the biosensor. EIS was a sensitive tool for observations of the differences on the working electrode surface during the building procedure of the immunosensor, and this technique was utilized to quantify the RBD antigen concentrations. Apart from the EIS technique, CV and SEM techniques were employed to characterize each sequential layer during the biosensor fabrication. The suggested design displayed a low detection limit (0.58 fg/mL) in a great linear detection range (0.0012−120 pg/mL) with acceptable recovery rates in nasal secretions. In addition, this biosensing system had long storage stability, good repeatability, and acceptable reproducibility. The outstanding features illustrated that the developed sensing system meets requirements for clinical diagnosis. Moreover, the designed immunosensor had good selectivity to the target analyte. The obtained results illustrated that the designed immunosensor was more sensitive than the other previously fabricated immunosensors. Furthermore, the usage of inexpensive ITO sheets as a biosensing platform for this immunosensor allowed low-cost biosensor production. The experimental results testified that the manufactured tool was accurate, convenient, and rapid. The high sensitivity and excellent specificity, ease of fabrication, operational simplicity, and reusability made this proposed immunosensor a promising candidate for determination of spike RBD, a precious marker of COVID-19 disease. Future studies could be attempted to develop portable electrochemical nanomaterial-polymer nanocomposite-based spike RBD biosensors. Thus, patients will be able to reach the result with on-site analysis without transmitting the pandemic disease to others.

ASSOCIATED CONTENT

Supporting Information

The Supporting Information is available free of charge at https://pubs.acs.org/doi/10.1021/acsbiomaterials.1c00580.

Materials and reagents, characterization and test equipment, chemical characterization of the monomer, repeatability result of the RBD biosensor, fitted EIS spectral results of electrode modification steps (A) and RBD antigen immobilized electrodes (B) (PDF)

AUTHOR INFORMATION

Corresponding Author

Mustafa Kemal Sezgintürk − *Bioengineering Department, Faculty of Engineering, Çanakkale Onsekiz Mart University, Çanakkale 17100, Turkey;* orcid.org/0000-0003-3042-1087; Email: msezginturk@hotmail.com

Authors

Elif Burcu Aydın − *Scientific and Technological Research Center, Tekirdağ Namık Kemal University, Tekirdağ 59030, Turkey*

Muhammet Aydın − *Scientific and Technological Research Center, Tekirdağ Namık Kemal University, Tekirdağ 59030, Turkey*

Complete contact information is available at: https://pubs.acs.org/10.1021/acsbiomaterials.1c00580

Notes

The authors declare no competing financial interest.

ACKNOWLEDGMENTS

The authors would like to acknowledge the financial support from The Scientific and Technological Research Council of Çanakkale Onsekiz Mart University, (FIA-2020-3304).

REFERENCES

(1) Zeng, L.; Li, Y.; Liu, J.; Guo, L.; Wang, Z.; Xu, X.; Song, S.; Hao, C.; Liu, L.; Xin, M. Rapid, ultrasensitive and highly specific biosensor for the diagnosis of SARS-CoV-2 in clinical blood samples. *Mater. Chem. Front.* **2020**, *4*, 2000−2005.

(2) Lai, C.-C.; Shih, T.-P.; Ko, W.-C.; Tang, H.-J.; Hsueh, P.-R. Severe acute respiratory syndrome coronavirus 2 (SARS-CoV-2) and coronavirus disease-2019 (COVID-19): The epidemic and the challenges. *Int. J. Antimicrob. Agents* **2020**, *55*, No. 105924.

(3) Gabutti, G.; d'Anchera, E.; Sandri, F.; Savio, M.; Stefanati, A. Coronavirus: update related to the current outbreak of COVID-19. *J. Infect. Dis. Ther.* **2020**, *9*, 241−253.

(4) Shi, R.; Shan, C.; Duan, X.; Chen, Z.; Liu, P.; Song, J.; Song, T.; Bi, X.; Han, C.; Wu, L. A human neutralizing antibody targets the receptor-binding site of SARS-CoV-2. *Nature* **2020**, *584*, 120−124.

(5) Chi, X.; Yan, R.; Zhang, J.; Zhang, G.; Zhang, Y.; Hao, M.; Zhang, Z.; Fan, P.; Dong, Y.; Yang, Y. A neutralizing human antibody binds to the N-terminal domain of the Spike protein of SARS-CoV-2. *Science* **2020**, *369*, 650−655.

(6) Benton, D. J.; Wrobel, A. G.; Xu, P.; Roustan, C.; Martin, S. R.; Rosenthal, P. B.; Skehel, J. J.; Gamblin, S. J. Receptor binding and priming of the spike protein of SARS-CoV-2 for membrane fusion. *Nature* **2020**, *588*, 327−330.

(7) Kang, S.; Yang, M.; Hong, Z.; Zhang, L.; Huang, Z.; Chen, X.; He, S.; Zhou, Z.; Zhou, Z.; Chen, Q. Crystal structure of SARS-CoV-2 nucleocapsid protein RNA binding domain reveals potential unique drug targeting sites. *Acta Pharm. Sin. B* **2020**, *10*, 1228−1238.

(8) Martin, W. R.; Cheng, F. Repurposing of FDA-approved toremifene to treat COVID-19 by blocking the Spike glycoprotein and NSP14 of SARS-CoV-2. *J. Proteome Res.* **2020**, *19*, 4670−4677.

(9) Mishra, S. Designing of cytotoxic and helper T cell epitope map provides insights into the highly contagious nature of the pandemic novel coronavirus SARS-CoV-2. *R. Soc. Open Sci.* **2020**, *7*, No. 201141.

(10) Cheng, Y.-W.; Chao, T.-L.; Li, C.-L.; Chiu, M.-F.; Kao, H.-C.; Wang, S.-H.; Pang, Y.-H.; Lin, C.-H.; Tsai, Y.-M.; Lee, W.-H. Furin inhibitors block SARS-CoV-2 spike protein cleavage to suppress virus production and cytopathic effects. *Cell Rep.* **2020**, *33*, No. 108254.

(11) Yakoh, A.; Pimpitak, U.; Rengpipat, S.; Hirankarn, N.; Chailapakul, O.; Chaiyo, S. Based electrochemical biosensor for diagnosing COVID-19: Detection of SARS-CoV-2 antibodies and antigen. *Biosens. Bioelectron.* **2021**, *176*, No. 112912.
(12) Carter, L. J.; Garner, L. V.; Smoot, J. W.; Li, Y.; Zhou, Q.; Saveson, C. J.; Sasso, J. M.; Gregg, A. C.; Soares, D. J.; Beskid, T. R., *Assay techniques and test development for COVID-19 diagnosis*; ACS Publications, 2020.
(13) Cui, F.; Zhou, H. S. Diagnostic methods and potential portable biosensors for coronavirus disease 2019. *Biosens. Bioelectron.* **2020**, *165*, No. 112349.
(14) Li, C.; Zhao, C.; Bao, J.; Tang, B.; Wang, Y.; Gu, B. Laboratory diagnosis of coronavirus disease-2019 (COVID-19). *Clin. Chim. Acta* **2020**, *510*, 35.
(15) Raziq, A.; Kidakova, A.; Boroznjak, R.; Reut, J.; Öpik, A.; Syritski, V. Development of a portable MIP-based electrochemical sensor for detection of SARS-CoV-2 antigen. *Biosens. Bioelectron.* **2021**, *178*, No. 113029.
(16) Mobed, A.; Shafigh, E. S. Biosensors promising bio-device for pandemic screening "COVID-19". *Microchem. J.* **2021**, *164*, No. 106094.
(17) Vadlamani, B. S.; Uppal, T.; Verma, S. C.; Misra, M. Functionalized TiO2 nanotube-based electrochemical biosensor for rapid detection of SARS-CoV-2. *Sensors* **2020**, *20*, 5871.
(18) Lee, J.-H.; Choi, M.; Jung, Y.; Lee, S. K.; Lee, C.-S.; Kim, J.; Kim, J.; Kim, N. H.; Kim, B.-T.; Kim, H. G. A novel rapid detection for SARS-CoV-2 spike 1 antigens using human angiotensin converting enzyme 2 (ACE2). *Biosens. Bioelectron.* **2021**, *171*, No. 112715.
(19) Mavrikou, S.; Moschopoulou, G.; Tsekouras, V.; Kintzios, S. Development of a portable, ultra-rapid and ultra-sensitive cell-based biosensor for the direct detection of the SARS-CoV-2 S1 spike protein antigen. *Sensors* **2020**, *20*, 3121.
(20) Mojsoska, B.; Larsen, S.; Olsen, D. A.; Madsen, J. S.; Brandslund, I.; Alatraktchi, F. A. Rapid SARS-CoV-2 Detection Using Electrochemical Immunosensor. *Sensors* **2021**, *21*, 390.
(21) Kaur, G.; Adhikari, R.; Cass, P.; Bown, M.; Gunatillake, P. Electrically conductive polymers and composites for biomedical applications. *RSC Adv.* **2015**, *5*, 37553−37567.
(22) Anantha-Iyengar, G.; Shanmugasundaram, K.; Nallal, M.; Lee, K.-P.; Whitcombe, M. J.; Lakshmi, D.; Sai-Anand, G. Functionalized conjugated polymers for sensing and molecular imprinting applications. *Prog. Polym. Sci.* **2019**, *88*, 1−129.
(23) Aydın, E. B.; Aydın, M.; Sezgintürk, M. K. Fabrication of electrochemical immunosensor based on acid-substituted poly (pyrrole) polymer modified disposable ITO electrode for sensitive detection of CCR4 cancer biomarker in human serum. *Talanta* **2021**, *222*, No. 121487.
(24) Kenry; Liu, B. Recent advances in biodegradable conducting polymers and their biomedical applications. *Biomacromolecules* **2018**, *19*, 1783−1803.
(25) Teles, F.; Fonseca, L. Applications of polymers for biomolecule immobilization in electrochemical biosensors. *Mater. Sci. Eng. C* **2008**, *28*, 1530−1543.
(26) Ibanez, J. G.; Rincón, M. E.; Gutierrez-Granados, S.; Chahma, M. H.; Jaramillo-Quintero, O. A.; Frontana-Uribe, B. A. Conducting polymers in the fields of energy, environmental remediation, and chemical−chiral sensors. *Chem. Rev.* **2018**, *118*, 4731−4816.
(27) Kaloni, T. P.; Giesbrecht, P. K.; Schreckenbach, G.; Freund, M. S. Polythiophene: from fundamental perspectives to applications. *Chem. Mater.* **2017**, *29*, 10248−10283.
(28) Huynh, T.-P.; Sharma, P. S.; Sosnowska, M.; D'Souza, F.; Kutner, W. Functionalized polythiophenes: Recognition materials for chemosensors and biosensors of superior sensitivity, selectivity, and detectability. *Prog. Polym. Sci.* **2015**, *47*, 1−25.
(29) Lock, J. P.; Im, S. G.; Gleason, K. K. Oxidative chemical vapor deposition of electrically conducting poly (3, 4-ethylenedioxythiophene) films. *Macromolecules* **2006**, *39*, 5326−5329.
(30) Haldar, R.; Sen, B.; Hurrle, S.; Kitao, T.; Sankhla, R.; Kühl, B.; Welle, A.; Heissler, S.; Brenner-Weiß, G.; Thissen, P. Oxidative polymerization of terthiophene and a substituted thiophene monomer in metal-organic framework thin films. *Eur. Polym. J.* **2018**, *109*, 162−168.
(31) Alshammary, B.; Walsh, F. C.; Herrasti, P.; de Leon, C. P. Electrodeposited conductive polymers for controlled drug release: polypyrrole. *J. Solid State Electrochem.* **2016**, *20*, 839−859.
(32) Zhang, D.; Li, L.; Ma, W.; Chen, X.; Zhang, Y. Electrodeposited reduced graphene oxide incorporating polymerization of l-lysine on electrode surface and its application in simultaneous electrochemical determination of ascorbic acid, dopamine and uric acid. *Mater. Sci. Eng. C* **2017**, *70*, 241−249.
(33) Gu, Y.; Wang, J.; Pan, M.; Li, S.; Fang, G.; Wang, S. Label-free impedimetric immunosensor based on one-step co-electrodeposited poly-(pyrrole-co-pyrrole-1-propionic acid) and reduced graphene oxide polymer modified layer for the determination of melamine. *Sens. Actuators B* **2019**, *283*, 571−578.
(34) Deng, P.; Xu, Z.; Feng, Y. Acetylene black paste electrode modified with graphene as the voltammetric sensor for selective determination of tryptophan in the presence of high concentrations of tyrosine. *Mater. Sci. Eng. C* **2014**, *35*, 54−60.
(35) Nezakati, T.; Seifalian, A.; Tan, A.; Seifalian, A. M. Conductive polymers: opportunities and challenges in biomedical applications. *Chem. Rev.* **2018**, *118*, 6766−6843.
(36) Sun, D.; Zhang, H. Electrochemical determination of 2-chlorophenol using an acetylene black film modified glassy carbon electrode. *Water Res.* **2006**, *40*, 3069−3074.
(37) Neises, B.; Steglich, W. Simple method for the esterification of carboxylic acids. *Angew. Chem. Int. Ed. Engl.* **1978**, *17*, 522−524.
(38) Aydın, M. A sensitive and selective approach for detection of IL 1α cancer biomarker using disposable ITO electrode modified with epoxy-substituted polythiophene polymer. *Biosens. Bioelectron.* **2019**, *144*, No. 111675.
(39) Raftery, L. J.; Grewal, Y. S.; Howard, C. B.; Jones, M. L.; Shiddiky, M. J.; Carrascosa, L. G.; Thurecht, K. J.; Mahler, S. M.; Trau, M. Biosensing made easy with PEG-targeted bi-specific antibodies. *Chem. Commun.* **2016**, *52*, 5730−5733.
(40) Ramvikas, M.; Arumugam, M.; Chakrabarti, S.; Jaganathan, K. Nasal vaccine delivery. In *Micro and Nanotechnology in Vaccine Development*; Elsevier: 2017; 279−301.
(41) Aydın, E. B.; Aydın, M.; Sezgintürk, M. K. Selective and ultrasensitive electrochemical immunosensing of NSE cancer biomarker in human serum using epoxy-substituted poly (pyrrole) polymer modified disposable ITO electrode. *Sens. Actuators B* **2020**, *306*, No. 127613.
(42) Tran, T.-N.; Di Mauro, C.; Graillot, A.; Mija, A. Monitoring the structure−reactivity relationship in epoxidized perilla and safflower oil thermosetting resins. *Poly. Chem.* **2020**, *11*, 5088−5097.
(43) Aydın, E. B.; Aydın, M.; Yuzer, A.; Ince, M.; Ocakoğlu, K.; Sezgintürk, M. K. Detection of Kallikrein-Related Peptidase 4 with a Label-free Electrochemical Impedance Biosensor Based on a Zinc (II) Phthalocyanine Tetracarboxylic Acid-Functionalized Disposable Indium Tin Oxide Electrode. *ACS Biomater Sci. Eng.* **2021**, *7*, 1192−1201.
(44) Aydın, E. B.; Aydın, M.; Sezgintürk, M. K. A novel electrochemical immunosensor based on acetylene black/epoxy-substituted-polypyrrole polymer composite for the highly sensitive and selective detection of interleukin 6. *Talanta* **2021**, *222*, No. 121596.
(45) Ghosh, A.; Raha, S.; Dey, S.; Chatterjee, K.; Chowdhury, A. R.; Barui, A. Chemometric analysis of integrated FTIR and Raman spectra obtained by non-invasive exfoliative cytology for the screening of oral cancer. *Analyst* **2019**, *144*, 1309−1325.
(46) Mishra, R. K.; Hayat, A.; Catanante, G.; Ocaña, C.; Marty, J.-L. A label free aptasensor for Ochratoxin A detection in cocoa beans: An application to chocolate industries. *Anal. Chim. Acta* **2015**, *889*, 106−112.
(47) Grewal, Y. S.; Shiddiky, M. J.; Gray, S. A.; Weigel, K. M.; Cangelosi, G. A.; Trau, M. Label-free electrochemical detection of an

Entamoeba histolytica antigen using cell-free yeast-scFv probes. *Chem. Commun.* **2013**, *49*, 1551−1553.
(48) Gopalan, A. I.; Lee, K.-P.; Ragupathy, D. Development of a stable cholesterol biosensor based on multi-walled carbon nanotubes−gold nanoparticles composite covered with a layer of chitosan−room-temperature ionic liquid network. *Biosens. Bioelectron.* **2009**, *24*, 2211−2217.
(49) Shamsipur, M.; Gholivand, M. B.; Ehzari, H.; Pashabadi, A.; Arkan, E.; Mansouri, K. Single frequency impedance strategy employed in rapid detection of leukemia cancer cells using an electrospun PES-nanofiber reinforced ternary composite-based cytosensor. *Electrochim. Acta* **2018**, *283*, 1498−1506.
(50) Riechelmann, H.; Deutschle, T.; Friemel, E.; Gross, H.; Bachem, M. Biological markers in nasal secretions. *Eur. Respir. J.* **2003**, *21*, 600−605.
(51) Lescure, F.-X.; Bouadma, L.; Nguyen, D.; Parisey, M.; Wicky, P.-H.; Behillil, S.; Gaymard, A.; Bouscambert-Duchamp, M.; Donati, F.; Le Hingrat, Q. Clinical and virological data of the first cases of COVID-19 in Europe: a case series. *Lancet Infect. Dis.* **2020**, *20*, 697−706.

https://doi.org/10.1021/acsbiomaterials.1c00580
ACS Biomater. Sci. Eng. 2021, 7, 3874−3885